Wake Integration for Three-Dimensional Flowfield Computations: Applications

David L. Hunt*
Aircraft Research Association, Bedford MK41 7PF, England, United Kingdom
Russell M. Cummings†
California Polytechnic State University, San Luis Obispo, California 93407
and
Michael B. Giles‡
Oxford University, Oxford OX1 3QD, England, United Kingdom

A momentum balance approach is used to extract lift and drag from flowfield computations for wings and wing/bodies in subsonic/transonic flight. The drag is decomposed into vorticity, entropy, and enthalpy components that can be related to the established engineering concepts of induced drag, wave and profile drag, and engine power and efficiency. This decomposition of the drag is useful in formulating techniques for accurately evaluating drag using computational fluid dynamics calculations or experimental data. A formulation for reducing the size of the region of the crossflow plane required for calculating the forces is developed using cutoff parameters for viscosity and entropy. This improves the accuracy of the calculations and decreases the computation time required to obtain the results. The improved method is applied to a variety of configurations, including an elliptic wing, the M6 wing, the W4 wing–body, the M165 wing–body–foreplane, and the Lockheed Wing A. The accuracy of the force calculations is related to various aspects, including the axial position of the downstream crossflow plane, grid type (structured or unstructured), grid density, flow regime (subsonic or transonic), and boundary conditions.

Nomenclature

AR = wing aspect ratio, $\equiv b^2/S_{ref}$
a = acoustic speed
b = wingspan
C_D = drag coefficient, $\equiv D/q_\infty S_{ref}$
C_L = lift coefficient, $\equiv L/q_\infty S_{ref}$
c = wing chord
D = drag (force parallel to freestream direction)
e = wingspan efficiency factor
H = stagnation enthalpy
L = lift (force perpendicular to freestream direction)
M = Mach number
p = pressure
q = dynamic pressure, $\equiv \frac{1}{2}\rho U^2$
R = universal gas constant
Re_c = Reynolds number, based on wing chord, $\equiv \rho_\infty U_\infty c/\mu_\infty$
S_{ref} = reference area, taken as the wing planform area
s = entropy
T = temperature
U = velocity
x, y, z = Cartesian coordinate system
α = angle of attack
γ = ratio of specific heats
ζ = streamwise vorticity
μ = dynamic viscosity
ρ = freestream density
ψ = stream function
∞ = freestream condition

Introduction

ACCURATELY predicting aerodynamic forces from numerical simulations has become a goal of computational fluid dynamics (CFD) researchers. Early attempts at accomplishing this involved integrating the pressure and skin friction over the surface of the body to calculate lift and drag (the computational equivalent of force measurements in wind tunnels). Surface pressure integration has met with difficulties because of the introduction of artificial smoothing and the need to approximate the curved surfaces of the body with flat facets. Calculation of the skin friction at the surface also presents difficulties because of the need to numerically approximate the velocity gradient. An alternative approach is to calculate the physical sources of the forces directly. This has led various researchers to look at applying experimental wake integration methods to CFD calculations; a survey of these experimental methods was recently prepared by Takahashi.[1]

A reformulation of the momentum balance equations for lift and drag has shown that wake–integral methods could be performed in the near field that were as accurate as the traditional far-field analysis methods.[2,3] These integral relations need to be validated and applied to a variety of cases, including both Euler and Navier–Stokes computations, to determine the effect of the numerical approach on the accuracy of the drag extraction.[4] Various contributing factors, such as the type of grid (structured or unstructured), the grid density in the wake region, the flow regime (subsonic or transonic), and boundary conditions, need to be evaluated for their influence on the accuracy of the force estimation. Once methods are developed that will make accurate lift and drag calculations possible, these procedures can be coupled with design optimization algorithms and used to reduce the total drag of full configurations (with wings, bodies, and engine nacelles), including power effects. It will then be possible to optimally design an aircraft for overall reduction in total drag.

Review of Theory

By using a momentum balance approach, a system of integrals has been developed that reduces the task of force computation to the integration of various flow parameters in a crossflow plane downstream of a body.[2,3] The lift of the body can be related to the streamwise vorticity in the far field as

$$L \approx \rho_\infty U_\infty \int \int y\zeta \, dy \, dz \qquad (1)$$

The drag can be found to be made up of three components related to the entropy (viscous and wave drag), total enthalpy (engine thrust addition), and vorticity/stream function (induced drag):

$$D \approx D_1 + D_2 + D_3 \qquad (2)$$

where

$$D_1 = p_\infty \int \int \frac{s}{R} \, dy \, dz, \qquad D_2 = -\rho_\infty \int \int \Delta H \, dy \, dz$$

$$D_3 = \frac{1}{2} \rho_\infty \int \int \psi\zeta \, dy \, dz \qquad (3)$$

These integral relationships, which were developed in Ref. 2, used a Trefftz–plane concept and the following assumptions: 1) the crossflow plane must be aligned perpendicular to the freestream velocity vector, 2) the plane must include both wingtips unless appropriate methods are used to compute the stream function/vorticity relationships in a half plane, and 3) the crossflow plane must be downstream of the aircraft. The third assumption creates practical limitations to the ability of the method to accurately predict the drag of a complex configuration (wing/fuselage/engine), in that the downstream crossflow plane may be far enough away from the lifting surfaces to have allowed a significant transfer of energy from D_3 to D_1 as a result of numerical dissipation. It may be useful, therefore, to place the crossflow plane relatively close to the trailing edge of the wing, which may cause the crossflow plane to include portions of the fuselage. The fuselage will affect the position and strength of the vorticity in the crossflow plane and lead to overpredicted values of lift, because lift is the integral of the product of vorticity and lateral position of the vorticity [see Eq. (1) and Ref. 2].

Implementation

Basic Concepts

For most CFD computations, there is no crossflow plane in the computational grid, and so the most natural approach for the evaluation of the crossflow force integrals is to adopt techniques from flow visualization. A crossflow cutting plane can be defined orthogonal to the freestream flow and at a fixed distance downstream of the aircraft (see Fig. 1). The nodes on the cutting plane are defined by the intersection of the plane and the edges of the three-dimensional grid, and all flow variables can be defined at the new nodes by linear interpolation along the cut edges. The nodes of the cutting planes can be connected into triangles, based on the relationship of the cutting plane to the original cells (see Fig. 2).

The next issue is the interpretation of the values obtained from the force integrals. Using CFD methods, it is possible to directly evaluate the aerodynamic forces on the aircraft using a numerical approximation of the surface integral. In practice, the effects of artificial smoothing corrupt the results. From a momentum balance approach, the surface integration and far-field integration results should match, but the effects of artificial smoothing also appear as entropy in the far field, which
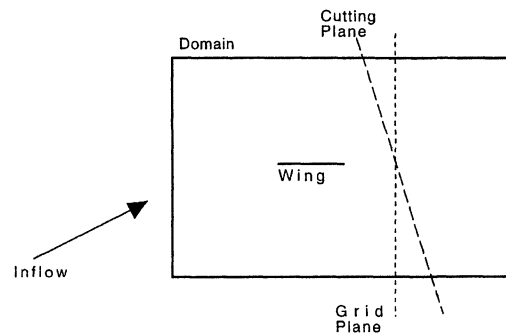

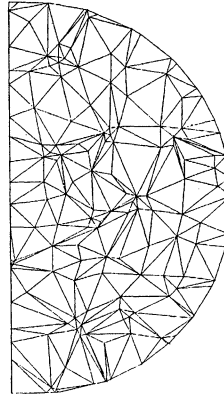Fig. 1 Cutting plane position within the computational domain.

Fig. 2 Typical wake crossflow half-plane.

was shown in the work of Wong et al.[5] They showed that the drag predicted by surface integration increased significantly as the level of artificial smoothing was increased. However, the crossflow plane integration for vortex drag was not greatly affected. It will be shown in the following sections that the contribution to entropy drag from the artificial smoothing can be minimized by analyzing the wake region with a downstream plane immediately aft of the wing.

Need for Cutoffs

A variety of practical issues arise when the momentum integrals for computing lift and drag [Eqs. (1–3)] are applied to either an experimental or computational set of data. Both experimentalists and computationalists want to reduce the size of the crossflow plane to reduce the time it takes to extract the forces. The wind-tunnel experimenter wants to decrease the size of the crossflow survey to reduce tunnel occupancy time, and the CFD user wants to be able to compute forces as quickly as possible, especially when using the computations in conjunction with a numerical optimization scheme. In the wind tunnel, the wake surveys are restricted to a crossflow plane the size of the test section. Further reduction in the probe survey size can be obtained by knowing that the wake, including the trailing vortices from the wing tips, lies in a fairly small region immediately behind the aircraft. It would be useful to be able to mimic this type of wake survey in the evaluation of drag using CFD results. The problem lies in determining when the crossflow plane is large enough to give accurate results.

In principle, it should be possible to integrate Eqs. (1–3) over the entire crossflow plane. However, initial applications of the crossflow plane integration to CFD results showed that nonphysical effects at the outer boundaries could contaminate the integration. Crossflow plane cells at the outer boundary are usually quite large, and so small errors near the outer boundary can lead to large errors in the integration. Integrations that were performed in Refs. 3 and 4 showed that forces such as lift could be in error by as much as 50% if the outer boundaries were included. Simply reducing the size of the crossflow plane so that the outer boundaries are excluded produced more accurate calculations of the lift and drag. However, further re-

ductions in the size of the crossflow plane continued to show improvements in accuracy until the crossflow plane became too small to include the wake region. Clearly, a method for reducing the size of the crossflow plane is required to improve the accuracy of the calculation, as well as to reduce the computational cost.

Cutoff Formulation (Elliptic Wing Case)

To show that the lift and drag of an aircraft could be accurately predicted using reduced crossflow plane sizes, a simple test case was run. An elliptic planform wing with aspect ratio of AR = 7, $M_\infty = 0.55$, and $\alpha = 4$ deg was chosen for this study (see Fig. 3). Euler computations were performed using the structured and unstructured numerical analysis (SAUNA) CFD system.[6,7] This wing has been computationally studied by Nikfetrat et al.[8] and van Dam and Nikfetrat[9]; computations were performed to match those cases. Crossflow planes were created from the flow solution using the flow visualization methods previously mentioned. The simplest method of reducing the size of the crossflow plane is to use a bounding box. A bounding box of N chords includes everything in the crossflow plane within a box outlined by $-N < y < +N$ and $-N < z < +N$ (where y and z are the lateral and vertical directions, respectively).

Figures 4 and 5 show the effect of the size of the bounding box on the computation of lift and drag. Figure 4 shows that the bounding box can be as small as three chords without affecting the prediction of lift, but that a bounding box that includes the outer boundary (14 chords) does not predict the lift accurately (as was explained in the previous section and reported in Ref. 4). In addition, the lift is consistently predicted with crossflow planes that are as much as seven chords behind the wing (discrepancies in the results at crossflow plane conditions aft of seven chords are a result of being in the proximity of the outflow boundary). The vortex drag (Fig. 5) is not significantly affected by the size of the bounding box, but the values do decrease as the crossflow plane is moved farther aft of the wing. This is because of numerical dissipation converting crossflow kinetic energy into entropy (D_3 to D_1).
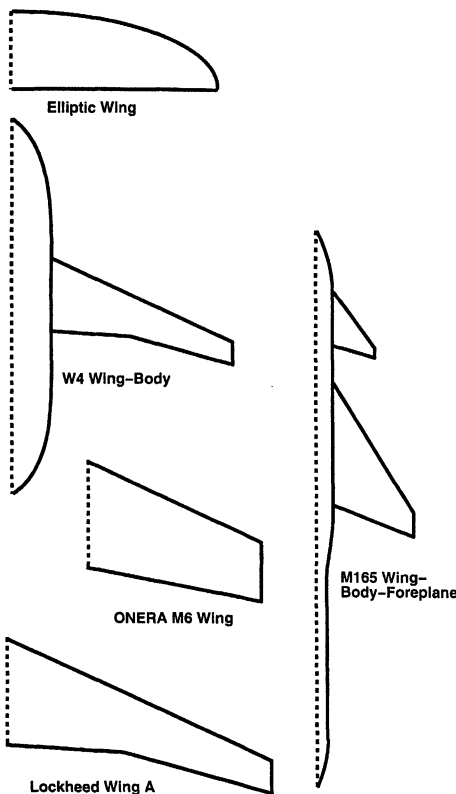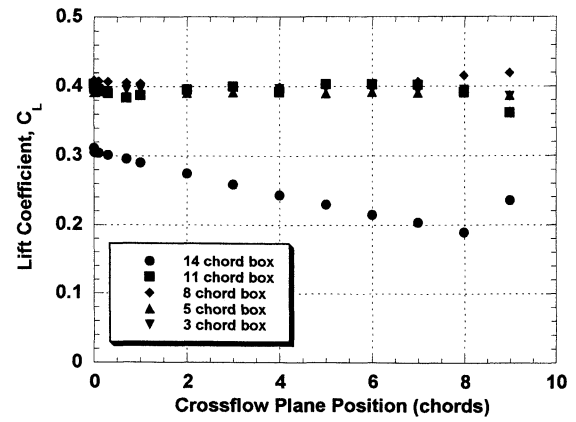

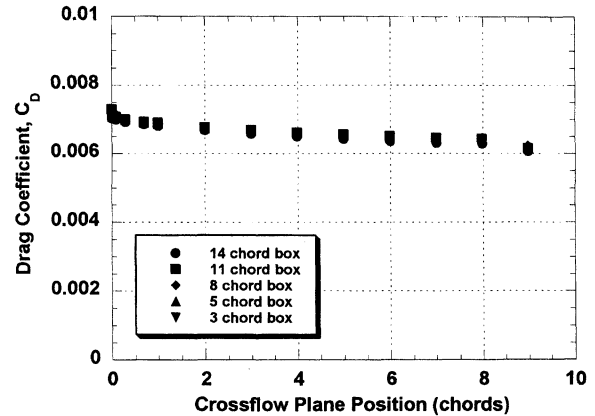Fig. 4   Elliptic wing, effect of bounding box size on lift coefficient.

Fig. 5   Elliptic wing, effect of bounding box size on vortex drag coefficient.

As mentioned in the previous section, the accuracy of the results can improve as the crossflow plane becomes smaller. When the crossflow plane is too large, the integration is corrupted by regions of vorticity and entropy that are not associated with the physical wake region. These regions of artificial vorticity and entropy are small in magnitude but can act over large area. These artificial effects are the result of numerical errors and artificial smoothing that are present in all CFD calculations. To optimize the accuracy of this technique, it is important that only the wake region is used to evaluate Eqs. (1–3), which leads to the need for a cutoff parameter.

A simple distance cutoff cannot accurately predict the shape of the wake, because the size of the wake is not known a priori. This indicates that there is a need for some other type of cutoff parameter to determine which cells contain significant levels of vorticity and which cells contain significant levels of entropy. Because the goal is for the integration to include only those cells that contain the wake, a cutoff parameter is needed to eliminate cells from the integration region if they have less than a certain level of entropy or vorticity.

A method for calculating these cutoff levels was developed that has proven to be robust over a range of flows.[4] Freestream levels of entropy and vorticity are defined using consistent dimensions: entropy with dimensions of energy per unit temperature and vorticity with dimensions of velocity per unit length. The reference parameters for the freestream level of entropy are the specific kinetic energy of the freestream, $U_\infty^2/2$, and the freestream temperature, T_∞. However, because $U_\infty^2 = M_\infty^2 a_\infty^2$ and $a_\infty^2 = \gamma R T_\infty$, the freestream entropy level can be expressed as

$$s_\infty = U_\infty^2/2T_\infty = (\gamma R/2)M_\infty^2 \qquad (4)$$

The freestream entropy level approximately represents the entropy increase that would occur if all the kinetic energy within
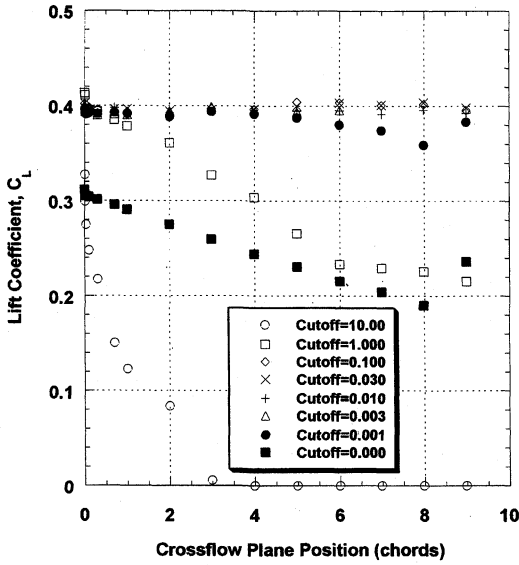

Fig. 3   Wing planforms.

Fig. 6 Elliptic wing, effect of level 1 cutoff parameter on lift coefficient.

Fig. 7 Elliptic wing, effect of level 1 cutoff parameter on vortex drag coefficient.

the fluid was turned into heat energy. The effect of both shock waves and boundary layers is to transfer kinetic energy to heat. Consequently, the wake region created by both boundary layers and shock waves will contain entropy at a level that is a significant proportion of the freestream entropy level. We may, therefore, expect this reference level to be appropriate for both types of wakes.

The reference parameters for the vorticity are defined as the freestream velocity and the wing semispan, $b/2$. The wing semispan is obtained from the definition of the AR, as $b/2 = \sqrt{S_{ref}AR}/2$, yielding the final reference level of

$$\zeta_\infty = 2U_\infty/\sqrt{S_{ref}AR} \tag{5}$$

The first entropy and vorticity cutoff parameters (level 1), C_{s_1} and C_{ζ_1}, are defined as threshold levels proportional to the freestream values, as given in Eqs. (4) and (5). The entropy or vorticity within a cell are not included in the wake if the levels of entropy or vorticity do not satisfy

$$s_{cell} > C_{s_1}s_\infty \tag{6}$$

$$|\zeta_{cell}| > C_{\zeta_1}\zeta_\infty \tag{7}$$

Because these cutoff levels are relative to the freestream values, they will be constant for all crossflow planes in the wake.

It has already been mentioned that some cells outside of the wake region have significant levels of entropy or vorticity because of numerical effects. If the force integration is performed with all of these cells (see Figs. 6 and 7), it can be seen that the lift integration can be consistently made with level 1 cutoff values for C_{ζ_1} between 0.001 and 0.1, but that cutoff values either above or below these levels seriously degrade the accuracy of the prediction. Problems occur below a cutoff of 0.001 because of the inclusion of cells outside the wake. The vortex drag is consistently predicted for cutoff values between 0 and 0.1, with poor predictions occurring for cutoff values above 0.1.

It is assumed that only the wake region will contain the largest values of entropy and vorticity, and so a second set of cutoff parameters (level 2) for the entropy and vorticity, C_{s_2} and C_{ζ_2}, are defined relative to the maximum values in each crossflow plane, s_{max} and ζ_{max}:

$$s_{cell} > C_{s_2}s_{max} \tag{8}$$
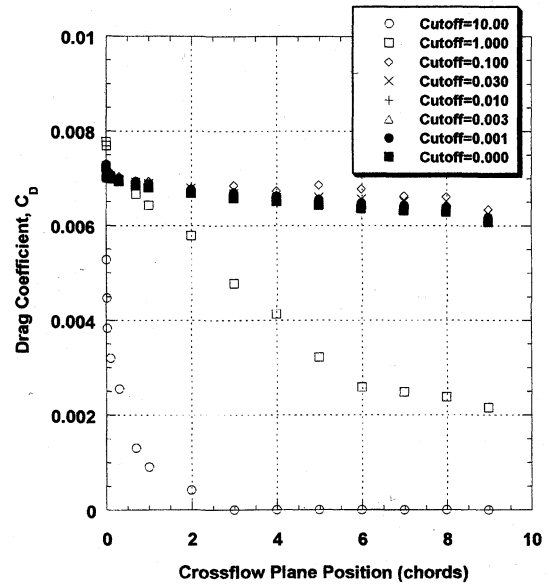
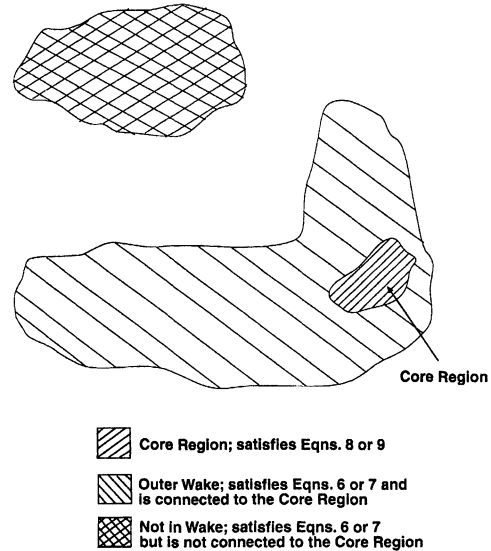$$|\zeta_{cell}| > C_{\zeta_2}\zeta_{max} \tag{9}$$

Fig. 8 Regions in crossflow plane.

Cells satisfying Eqs. (8) or (9) form the core region of the wake. The force integration is performed over these cells and the cells satisfying Eqs. (6) or (7) if they touch the core region of the wake, or are connected to the core region via other cells satisfying Eqs. (6) or (7), as shown in Fig. 8. This condition may be too restrictive for a complex configuration that produces two or more distinct wake regions, but it has proven to be adequate for the range of configurations considered to date, such as for the M165 wing–body–foreplane configuration. The resulting cutoff values vary between different crossflow planes in the wake. The values of maximum vorticity and entropy tend to decrease downstream of the configuration as artificial smoothing diffuses the wake. For this reason, this method may become less effective as the crossflow plane is moved downstream. Values of the various cutoff parameters were determined from computations using the elliptic wing.

While Figs. 6 and 7 show the variation of lift and vortex drag coefficients for various values of C_{ζ_1}, Figs. 9 and 10 show the results with two vorticity cutoff values, a level 1 value that varies as shown, and a constant level 2 value of $C_{\zeta_2} = 0.1$. These results show that the lift and vortex drag are consistently predicted for all combinations of cutoff values and at crossflow
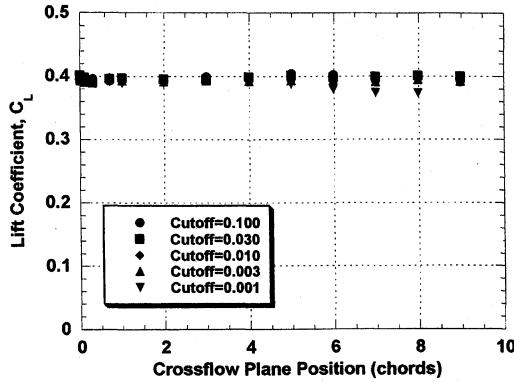
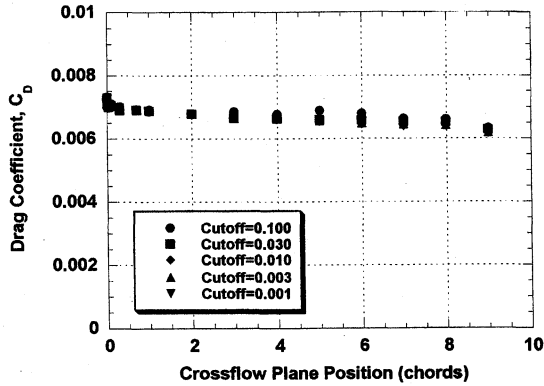Fig. 9 Elliptic wing, effect of level 1 cutoff parameter on lift coefficient; $C_{\zeta_2} = 0.1$.

Fig. 10 Elliptic wing, effect of level 1 cutoff parameter on vortex drag coefficient; $C_{\zeta_2} = 0.1$.

Table 1 Elliptic wing force comparisons; $M_\infty = 0.55$, $\alpha = 4$ deg

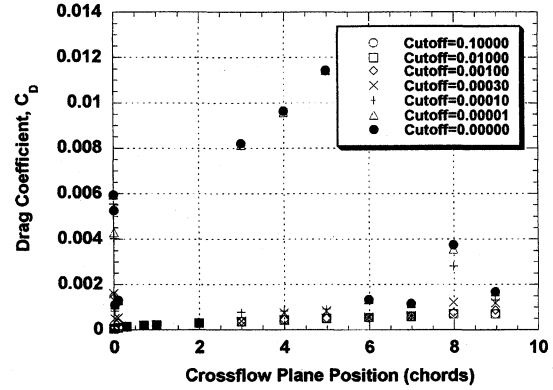| Integration	C_L	C_D	L/D
Wake	0.3918	0.00706	55.46
Wake[8]	0.3917	0.00704	55.64
Surface	0.3910	0.00810	48.27
Surface[8]	0.3914	0.00924	42.36

Fig. 11 Elliptic wing, effect of level 1 cutoff parameter on entropy drag coefficient; $C_{\zeta_2} = 0.1$.
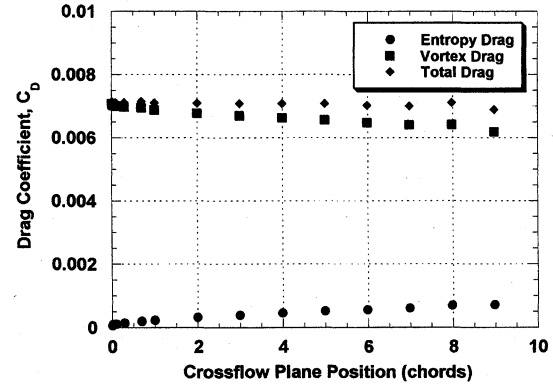

Fig. 12 Elliptic wing drag coefficient; $C_{\zeta_1} = 0.01$, $C_{\zeta_2} = 0.1$, $C_{s_1} = 0.003$, and $C_{s_2} = 0.1$.

plane positions within six chords of the wing. This leads to default values for the two vorticity cutoff parameters of $C_{\zeta_1} = 0.01$ and $C_{\zeta_2} = 0.1$. A similar determination of the entropy cutoff values (Fig. 11) shows that the entropy drag is consistently predicted for cutoff values of $C_{s_1} = 0.003$ and $C_{s_2} = 0.1$.

Results for the elliptic wing with the newly determined cutoff values are presented in Fig. 12 and Table 1. These show the entropy, vortex, and total drag coefficients as a function of streamwise position downstream of the wing (in chord lengths). When the default levels of cutoff values are applied to the total drag estimation, various interesting, but not unexpected, results take place. First of all, the total drag does not vary a great deal at various positions downstream of the wing (total drag in the wake should be invariant, as discussed in Refs. 2–4). The vortex drag continuously decreases as the crossflow plane is moved downstream, and the entropy drag continuously increases. This is the interchange of vorticity for entropy that is caused by numerical dissipation as the vortex convects downstream. It is because of this transfer of drag that the near field is the best place for computation of drag from CFD results. This shows that the crossflow plane integral formulation, which was developed for use in the far field, is valid in the near field.

The resulting lift and drag coefficients are $C_L = 0.3918$ and $C_D = 0.007064$, respectively (from averaged values for all crossflow plane positions from one to eight chords behind the wing). The wing geometry was used because of its elliptic spanwise lift distribution (the elliptic lift distribution of the wing was verified in Ref. 9), which means that the results of lifting-line theory should be relatively accurate: $C_D = C_L^2/\pi e AR$, where $e = 1.0$ for a wing with an elliptic distribution of lift and a planar wake. The induced drag coefficient resulting from lifting line theory is $C_D = 0.006978$ (for $C_L = 0.3918$); the computed value is within ~1% of the lifting-line result. If the drag is computed by integrating pressures over the surface of the wing, the result is $C_D = 0.00810$, which is

about 15% higher than the results from wake integration. Similar trends were obtained in Ref. 8, where the differences between the surface integration and wake analysis were attributed to numerical viscosity, which is added in Euler codes. The numerical viscosity that leads to this artificial drag contribution creates entropy that should appear in the wake. The fact that it does not appear in the entropy integral is a result of the entropy integral being evaluated over the physical wake region. This indicates that the entropy caused by the artificial drag component is spread over a much wider region of the crossflow plane than the physical wake extracted in this analysis. In effect, the process of wake extraction for the elliptic wing filters out most of the drag contribution caused by artificial smoothing within the CFD solution.

Applications

To assess the robustness of the wake analysis described in the previous section, it has been applied to a number of Euler and Navier–Stokes test cases. Experimental values are provided for reference. In all these cases, the entropy and vorticity cutoffs were set to the default values that had been developed for the elliptic wing; $C_{\zeta_1} = 0.01$, $C_{\zeta_2} = 0.1$, $C_{s_1} = 0.003$, and $C_{s_2} = 0.1$.

M6 Wing

Calculations were performed on the ONERA M6 Wing[10] (see Fig. 3) for $M_\infty = 0.84$ and $\alpha = 6.06$ deg, using both structured and unstructured grids. The structured grid contained 189,000 points, and the unstructured grid contained 98,000 nodes and 576,000 cells. Note that the densities of the two grid types do not match because the computations were performed with different Euler codes: the structured grid used the SAUNA code[6,7] and the unstructured grid used the Cindy code.[11] Interpretation of results and conclusions need to be made with care because of the differences in grid density levels between the structured and unstructured cases.

Detailed results for the M6 wing can be found in Ref. 4, where comparisons between the structured and unstructured grids of different density are shown for lift, entropy drag, and vortex drag. The results show that the lift predicted by both grids are consistent with the corresponding values obtained using surface integration. The wake integration results for the structured and unstructured fine grids are compared in Figs. 13 and 14, respectively, and Table 2. While the total drag is fairly constant for both grid types, there is an obvious exchange of vortex drag for entropy drag as the crossflow plane is moved farther downstream. However, this trend stops after five chord lengths for the structured grid, but continues farther downstream for the unstructured grid.

The differences in predicted lift and drag between the two grid types can be attributed to the fact that at this Mach number two shocks form on the inboard section of the wing, one slightly aft of the leading edge and one slightly before the trailing edge. Farther outboard on the wing, the shocks coalesce to form a single, nearly normal shock. The spanwise location and strength of the shock intersection is very sensitive to a number of factors, including the grid density in the vicinity of the shock, the dissipation scheme, and possibly the grid type (structured or unstruct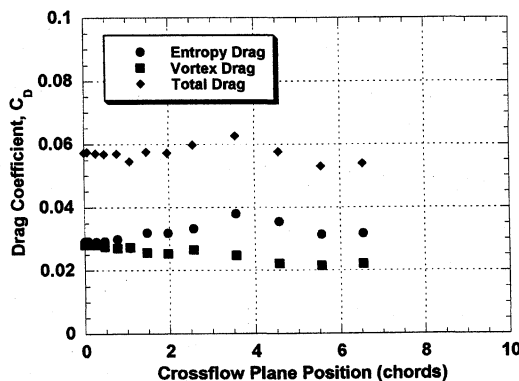ured). The accuracy of the prediction of this complex, three-dimensional shock structure has a large impact on the prediction of wave drag. The resulting lift-to-drag ratio for the structured fine grid is $L/D = 10.44$, whereas the unstructured fine grid yields $L/D = 9.153$, a difference of ~12%. Unfortunately, no force data were taken in the experimental evaluation of the M6 wing in Ref. 10. Surface pressure integration shows more consistent results than the elliptic wing case, with wake and surface results being within 3% of each other.

W4 Wing-Body

The W4 configuration is a civil transport wing–body (see Fig. 3), which shows the ability of the method to handle drag estimation for a geometry that includes the presence of a fuselage. The wing has an AR of 8 and was experimentally tested at $M_\infty = 0.78$ and $\alpha = 1.523$ deg.[12] Euler computations were made to match these conditions using the SAUNA code.[6,7]

Cutting planes taken immediately behind the wing will include part of the fuselage. The effect of doing this was discussed in Ref. 2. The W4 wing–body geometry was run without any fuselage correction to determine the feasibility of predicting drag from a cutting plane in the region of the fuselage.

A study of the grid density in the wake of the wing was also conducted. Three grids were tested, each with a different number of axial planes aft of the wing: 13, 27, and 37 planes. The entropy drag results for these three cases are presented in Fig. 15. The entropy drag results are fairly scattered for the grids that contain 13 and 27 planes, with a smoother variation of entropy drag for the grid with 37 wake planes. The vortex drag results are not shown because they are all identical (see Ref. 4 for details). The vortex drag is well predicted by all three wake grid sizes, showing that the vortex drag (and therefore the lift) requires much lower grid density in the wake to give accurate and consistent results. The prediction of entropy drag in the wake, however, requires higher levels of grid density.

The resulting values of entropy, vortex, and total drag are shown in Fig. 16 and Table 3. It should be kept in mind that the effects of viscous drag are not included in the CFD analysis. It is for this reason that the experimental value of drag is significantly higher than the predicted values. These results use the grid with 37 planes in the wake. The results show similar trends to the previous cases: an interchange of vortex and entropy drag, with a resulting total drag that is nearly constant throughout the wake. The average drag coefficient in

Fig. 13   M6 wing drag coefficient; structured grid; $C_{\xi_1} = 0.01$, $C_{\xi_2} = 0.1$, $C_{s_1} = 0.003$, and $C_{s_2} = 0.1$.
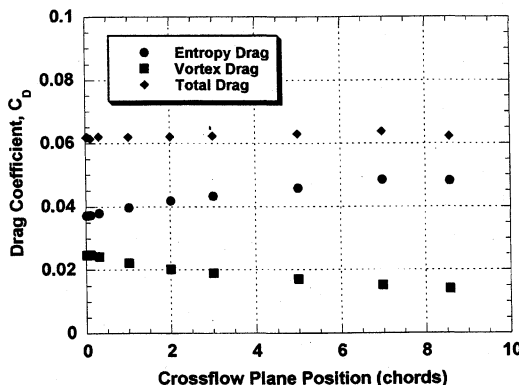
Table 2   M6 wing force comparisons; $M_\infty = 0.84$, $\alpha = 6.06$ deg

Integration	C_L	C_D	L/D
Surface: structured grid	0.5890	0.05540	10.63
Wake: structured grid	0.5953	0.05704	10.44
Surface: unstructured grid	0.5635	0.06552	8.60
Wake: unstructured grid	0.5700	0.06226	9.15

Fig. 14   M6 wing drag coefficient; unstructured grid; $C_{\xi_1} = 0.01$, $C_{\xi_2} = 0.1$, $C_{s_1} = 0.003$, and $C_{s_2} = 0.1$.
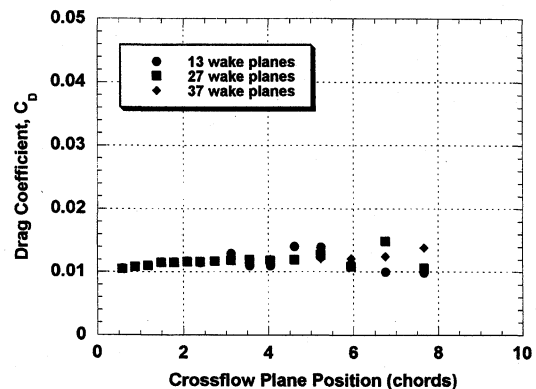

Fig. 15   W4 wing–body, effect of wake grid density on entropy drag coefficient; $C_{\xi_1} = 0.01$, $C_{\xi_2} = 0.1$, $C_{s_1} = 0.003$, and $C_{s_2} = 0.1$.

Table 3   W4 wing–body force comparisons; $M_\infty = 0.78$, $\alpha = 1.523$ deg

Force method	C_L	C_D	L/D
Wake integration	0.7508	0.03434	21.9
Surface integration	0.7490	0.03480	21.5
Experimental data[12]	0.7320	0.05202	14.1

Table 4   M165 wing–body–foreplane force comparisons; $M_\infty = 0.9$, $\alpha = 6$ deg

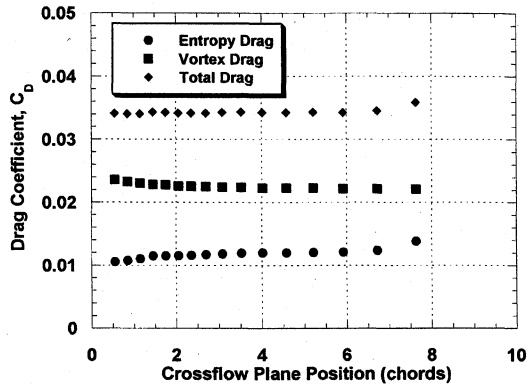| Force method	C_L	C_D	L/D
Wake integration	0.4358	0.03337	13.1
Surface integration	0.4260	0.03190	13.4
Experimental data[13]	0.3800	0.03800	10.0

Fig. 16   W4 wing–body drag coefficient; $C_{\xi_1} = 0.01$, $C_{\xi_2} = 0.1$, $C_{s_1} = 0.003$, and $C_{s_2} = 0.1$.

Table 5   Lockheed Wing A force comparisons; $M_\infty = 0.82$, $\alpha = 1.5$ deg, $Re_c = 6.0 \times 10^6$

Force method	C_L	C_D	L/D
Wake integration	0.4718	0.0323	14.6
Surface integration[15]	0.5160	0.0333	15.5
Experimental data[14]	0.5300	0.0395	13.4

Fig. 17   M165 canard–wing drag coefficient; $C_{\xi_1} = 0.01$, $C_{\xi_2} = 0.1$, $C_{s_1} = 0.003$, and $C_{s_2} = 0.1$.
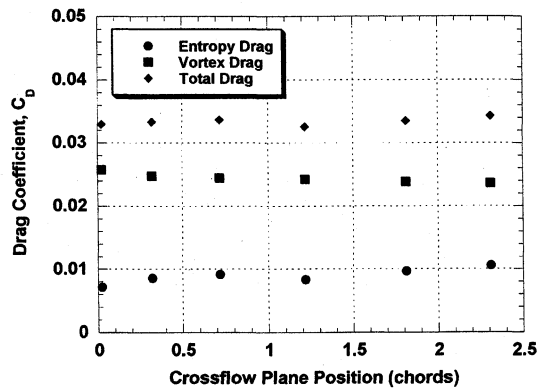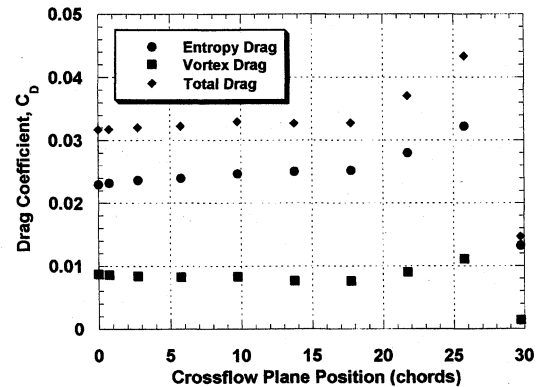

Fig. 18   Lockheed wing A drag coefficient; $C_{\xi_1} = 0.01$, $C_{\xi_2} = 0.1$, $C_{s_1} = 0.003$, and $C_{s_2} = 0.1$.

the wake is $C_D = 0.03434$, with a corresponding lift coefficient of $C_L = 0.7508$, which is also constant throughout the wake. The wake integration results are within about 1% of the surface integration results.

M165 Wing–Body–Foreplane

The M165 configuration is a simple wing–body–foreplane (see Fig. 3), which shows the effect of computing forces on multiple lifting surfaces located at different longitudinal positions in the configuration. The configuration has an aspect ratio of AR = 2.1 and was wind tunnel tested at $M_\infty = 0.9$ and $\alpha = 6$ deg.[13] Euler computations from the SAUNA code[6,7] were made to match the experimental case.

The crossflow plane is positioned at various locations behind the trailing edge of the wing. Because the wing is behind the foreplane, the transfer of vortex drag to entropy drag for the foreplane has already begun to take place at the position of the wing. In spite of this, the results in Fig. 17 and Table 4 show that the overall drag of the configuration is consistently predicted (with an average value of $C_D = 0.03337$), with the majority of the total coming from vortex drag. The interchange between vortex drag and entropy drag is also apparent for this case.

As with the W4 wing–body case, the wake and surface integration results are very close to one another. The foreplane vortex passes over the top of the wing and remains separate from the wing vortex. There is, however, a low level of vor-

ticity shed from the body that connects the two vortex wakes. The results indicate that the wake extraction algorithm has been able to extract the wake caused by both lifting surfaces. Again, because the effects of viscous drag are not included in the CFD analysis the experimental value of drag is higher than the predicted values. The discrepancy between the experimental and CFD lift results can be partly attributed to the fact that the rear of the geometry was modified from that used in the experimental case to facilitate its use in the CFD code, and partly because of the absence of viscous effects in the Euler simulation.

Lockheed Wing A

To investigate the viability of the wake analysis method for a viscous calculation, a Navier–Stokes solution is considered. The Lockheed Wing A has a planform that is representative of an advanced commercial transport wing and was extensively wind-tunnel tested by Hinson and Burdges[14] (see Fig. 3). The wing has an AR = 8, a taper ratio of 0.4, a leading-edge sweep of 27 deg, and uses a 12% thick airfoil that is continuously twisted from the root to the tip. The wing flowfield was computed by Greenman et al.,[15] using the OVERFLOW compressible Navier–Stokes solver[16] with a single-zone structured grid. The computations were made at $M_\infty = 0.82$, $\alpha = 1.5$ deg, and $Re_c = 6.0 \times 10^6$.

It can be seen from Table 5 that the lift has been underpredicted; it is not clear why this discrepancy occurs. As in the previous cases, the elliptic wing cutoffs were found to give the best results. Figure 18 shows the entropy, vortex, and total drag for Wing A. These results show trends that are similar to previous results for the various inviscid cases, namely that the total drag is constant for as much as 20 chords downstream of the wing. The effects of the outflow boundary then begin to contaminate the crossflow plane data and cause inaccuracies in the results. The entropy drag is seen to increase throughout

much of the wake, with a corresponding decrease in vortex drag.

Recommendations

Several recommendations for accurate prediction of drag can be made based on the results of the test cases:

1) Studies should be conducted to investigate how grid resolution affects the quality of the results.

2) Studies should be conducted to investigate the ability of far-field drag methods to predict incremental drag over small changes in flow conditions and geometry.

3) Wake integration should be performed using the near-field integrals [Eqs. (1–3)] with crossflow planes as close to the aft of the body as possible to minimize the effects of vortex drag shifting to entropy drag caused by numerical dissipation.

4) Crossflow planes should not include cells that are near outer boundaries of the computational domain.

5) Numerical methods with minimal artificial viscosity should be used for drag prediction, or explicitly added artificial viscosity should be used and corrected.[17]

6) The application of this method to viscous cases requires further development.

The current methods have been applied to a variety of inviscid and viscous cases to determine the levels of the cutoff parameters for consistent prediction of lift and drag. Further applications of these concepts to more complex geometries may lead to the accurate and efficient extraction of forces from CFD computations.

Conclusions

A previously developed wake integral formulation for the prediction of lift and drag (both entropy drag and vortex drag) has been used on a variety of test cases. Methods for reducing the computational time required for integrating the wake crossflow planes are implemented so that the process can be utilized in conjunction with numerical optimization algorithms. This is achieved by cutting out the wake region. The wake region is defined as consisting of cells with entropy or vorticity above a reference level that are contiguous with the region where entropy or vorticity is largest.

Cutting out the wake region was found to be essential to the accuracy of the wake integral method when applied to realistic configurations. It was also shown that by efficiently cutting out the wake region, it is possible to filter out a proportion of the contribution to entropy drag from artificial viscosity. It was found that this method was able to accurately predict lift for Euler calculations, and predicted a total drag that was comparable or better than the value obtained from surface pressure integration. The ability to separate the total drag into an entropy and vortex component was not straightforward because of the dissipation of the vortex system downstream of the configuration. Also, while lift and vortex drag are well predicted, even with coarse grids in the wake region, entropy drag (wave and/or profile drag) requires higher grid density in the wake region.

Acknowledgments

References

[1]Takahashi, T. T., "On the Decomposition of Drag from Wake Survey Measurements," AIAA Paper 97-0717, Jan. 1997.

[2]Giles, M. B., and Cummings, R. M., "Wake Integration for Three-Dimensional Flowfield Computations: Theoretical Development," *Journal of Aircraft*, Vol. 36, No. 2, 1999, pp. 357–365.

[3]Cummings, R. M., Giles, M., and Shrinivas, G., "Analysis of the Elements of Drag in Three-Dimensional Viscous and Inviscid Flows," AIAA Paper 96-2482, June 1996.

[4]Hunt, D. L., Cummings, R. M., and Giles, M. B., "Determination of Drag from Three-Dimensional Viscous and Inviscid Flowfield Computations," AIAA Paper 97-2257, June 1997.

[5]Wong, K. J., Ayers, T. K., and Van Dam, C. P., "Accurate Drag Prediction—A Prerequisite for Drag Reduction Research," Society of Automotive Engineers, Paper 932571, Sept. 1993.

[6]Shaw, J. A., Peace, A. J., Georgala, J. M., and Childs, P. N., "Validation and Evaluation of the Advanced Aeronautical CFD System SAUNA—A Method Developer's View," European Forum on Recent Development and Application in Aeronautical CFD, Bristol, England, UK, 1993.

[7]Shaw, J. A., Peace, A. J., May, N. E., and Pocock, M. K., "Verification of the CFD Simulation System SAUNA for Complex Aircraft Configurations," AIAA Paper 94-0393, Jan. 1994.

[8]Nikfetrat, K., Van Dam, C. P., Vijgen, P. M. H. W., and Chang, I. C., "Prediction of Drag at Subsonic and Transonic Speeds Using Euler Methods," AIAA Paper 92-0169, Jan. 1992.

[9]Van Dam, C. P., and Nikfetrat, K., "Accurate Prediction of Drag Using Euler Methods," *Journal of Aircraft*, Vol. 29, No. 3, 1992, pp. 516–519.

[10]Schmitt, V., and Charpin, F., "Pressure Distribution on the ONERA-M6-Wing at Transonic Mach Numbers," AGARD AR-138, May 1979.

[11]Crumpton, P. I., "An Efficient Cell Vertex Method for Unstructured Tetrahedral Grids," *Numerical Methods for Fluid Dynamics V*, edited by K. W. Morton and M. J. Baines, Clarendon, Oxford, England, UK, 1995, pp. 369–376.

[12]Fulker, J. L., "A Selection of Experimental Test Cases for the Validation of CFD Codes—Case B3," AGARD AR 303, Aug. 1994.

[13]Stanniland, D. R., "A Selection of Experimental Test Cases for the Validation of CFD Codes—Case D," AGARD AR 303, Aug. 1994.

[14]Hinson, B. L., and Burdges, K. P., "Acquisition and Application of Transonic Wing and Far-Field Test Data for Three-Dimensional Computational Method Evaluation," U.S. Air Force Office of Scientific Research, TR-80-0421, March 1980.

[15]Greenman, R. M., Cheung, S., and Tu, E. L., "Optimization: A Tool to Study the Physical Features of a Transonic Wing," AIAA Paper 96-2486, June 1996.

[16]Buning, P. G., Chan, W. M., Renze, K. J., Sondak, D. L., Chiu, I. T., and Slotnick, J. P., "OVERFLOW Manual Version 1.6ab," NASA Ames Research Center, Moffett Field, CA, Jan. 1993.

[17]Varma, R. R., and Caughey, D. A., "Evaluation of Navier-Stokes Solutions Using the Integrated Effect of Numerical Dissipation," *AIAA Journal*, Vol. 32, No. 2, 1994, pp. 294–300.